CARBON 69 (2014) 92–100

Available at www.sciencedirect.com

ScienceDirect

journal homepage: www.elsevier.com/locate/carbon

C_{60} aminofullerene-magnetite nanocomposite designed for efficient visible light photocatalysis and magnetic recovery

Yeoseon Choi [a,1], Youngjin Ye [a,1], Yuri Mackeyev [b], Min Cho [c], Sanghyup Lee [e,f], Lon J. Wilson [b], Jinwoo Lee [a], Pedro J.J. Alvarez [d], Wonyong Choi [a,*], Jaesang Lee [e,*]

[a] Chemical Engineering, Pohang University of Science and Technology (POSTECH), Pohang 790-784, South Korea
[b] Chemistry, Smalley Institute for Nanoscale Science and Technology, Rice University, Houston, TX 77005, United States
[c] Biotechnology, Chonbuk National University, Iksan 570-752, South Korea
[d] Civil and Environmental Engineering, Rice University, Houston, TX 77005, United States
[e] Water Resource Cycle Center, Korea Institute of Science and Technology, Seoul 136-791, South Korea
[f] Graduate School of Convergence Green Technology and Policy, Korea University, Seoul 136-701, South Korea

ARTICLE INFO

Article history:
Received 12 October 2013
Accepted 26 November 2013
Available online 4 December 2013

ABSTRACT

A magnetically recyclable photosensitizing system for harnessing solar energy for water treatment and disinfection is reported. This system comprises C_{60} aminofullerene as a sensitizer for singlet oxygenation and functionalized mesoporous silica (msu-f SiO_2) encapsulating magnetite nanoparticles (msu-SiO_2/mag) as a magnetically separable host. Rapid degradation of furfuryl alcohol (FFA) (a singlet oxygen ($^1O_2$) probe) under visible-light irradiation along with the kinetic retardation of FFA decomposition in the presence of $^1O_2$ quenchers suggests that the visible-light activity of C_{60} aminofullerene-derivatized msu-SiO_2/mag (C_{60}/msu-SiO_2/mag) is related to the photosensitization of $^1O_2$. On the other hand, the use of SiO_2 gel and fumed SiO_2 as magnetic supports drastically reduced the photosensitized generation of $^1O_2$, which is ascribed to the absence of an ordered pore structure in the alternative silica support, resulting in an uncontrolled growth of Fe_3O_4 and an aggregation of the fullerenes on the SiO_2 gel and fumed SiO_2. Significant $^1O_2$ production using C_{60}/msu-SiO_2/mag led to the effective oxidation of emerging pharmaceutical contaminants and inactivation of MS-2 bacteriophage under visible-light irradiation. Magnetic recovery and the subsequent reuse of the composite did not cause any significant loss in the photosensitizing activity of C_{60}/msu-SiO_2/mag, demonstrating its potential for catalytic applications.

1. Introduction

Photo-induced energy and electron transfer processes involving carbon-based nanomaterials (e.g., fullerenes, carbon nanotubes, and graphenes) have been attracting attention in the development of solar-powered systems for environmental remediation and renewable energy generation [1–4]. C_{60} fullerene is a carbonaceous nanomaterial that is photochemically activated under visible-light irradiation to produce singlet oxygen ($^1O_2$) with high quantum efficiency [5–7], enabling effective sensitized oxidation of organic pollutants and inactivation of viruses with relatively low energy input.

* *Corresponding authors:* Tel.: +82 2 958 6947; fax: +82 2 958 5839.
E-mail address: lee39@kist.re.kr (J. Lee).
[1] These authors contributed equally to this work.
0008-6223/$ - see front matter
http://dx.doi.org/10.1016/j.carbon.2013.11.065

However, the potential application of fullerene as an environmental photocatalyst in water treatment and disinfection processes is limited owing to the surface hydrophobicity of C_{60} [8]. Strategies for increasing the availability of C_{60} for aqueous-phase applications include: (1) the formation of water-stable colloidal C_{60} using ultrasonic radiation [9]; (2) the encapsulation of C_{60} in surfactant micelles [10]; and (3) the surface modification of C_{60} with hydrophilic functional groups [11,12]. In particular, the attachment of multiple hydrophilic addends allows the aqueous solubilization of C_{60} without a significant loss of photosensitizing activity [13,14] or secondary contamination with the dispersants [14].

Previous studies [15,16] have demonstrated the capability of water-soluble C_{60} derivatives to inactivate viruses based on the effective oxidation of the capsid proteins using photochemically generated $^1O_2$. Owing to the high susceptibility of electron-rich chemical moieties (e.g., conjugated double bonds and aromatic rings) to singlet oxygenation, surface-functionalized C_{60} achieves a rapid oxidative degradation of the selected organic compounds (e.g., chlorophenols and pharmaceuticals) under visible-light irradiation [17,18]. On the other hand, a nanoscale dispersion of C_{60} derivatives in water hinders their use as a visible-light-responsive photocatalyst, and causes an unwanted release of fullerenes into the environment [19,20]. Therefore, in order to achieve practical applications of photosensitized water remediation using C_{60}, it is necessary to develop a feasible approach to facilitate the recovery of functionalized C_{60} from the treated water.

A physical separability test confirmed the easy removal of amine-functionalized C_{60} immobilized on silica gel after it was used for the photosensitized oxidation of organic substances [18,21]. However, any industrial filtration process requires a continual supply of electricity. The magnetic removal of the adsorbents and photocatalysts composited with magnetic materials has been frequently investigated because such a process can be performed with a minimal use of energy and this approach can be employed for the development of an easily reusable and recoverable C_{60}-based photocatalyst. In order to fabricate a magnetically separable photosensitizer with visible-light activity, we report herein immobilization of C_{60} aminofullerene through the formation of a covalent linkage on functionalized mesoporous mesocellular silica (msu-SiO_2) embedded with magnetite nanoparticles. The msu-SiO_2 encapsulating Fe_3O_4 nanoparticles (msu-SiO_2/mag) shows the potential for fabricating magnetically recoverable systems of biological molecules and inorganic nanoparticles owing to a large surface area, high pore volume, and enhanced magnetic separability [22,23], implying the possible use as a magnetically separable host for C_{60} immobilization. By comparing msu-SiO_2 with SiO_2 gel and fumed SiO_2, this study has demonstrated the superiority of msu-SiO_2 as a support for a C_{60} aminofullerene-magnetite composite for visible-light photocatalysis. The photosensitizing activity of C_{60}/msu-SiO_2/mag has been evaluated in terms of (1) efficiency in a photosensitized $^1O_2$ yield; (2) recycling performance as a magnetic photocatalyst; and (3) kinetics for visible-light-induced oxidation of organic compounds and inactivation of virus.

2. Experimental

2.1. Preparation of 3-(2-succinic anhydride)propyl functionalized magnetic silica

Mesoporous mesocellular SiO_2 was synthesized according to previously reported methods [24,25]. SiO_2 gel (Devisil Grade 636) and fumed SiO_2 with an average particle size of 0.2–0.3 μm (S5505) were obtained from Sigma–Aldrich. 3-(Triethoxysilyl)propylsuccinic anhydride (TPSA) was obtained from Gelest. The SiO_2 gel and fumed SiO_2 impregnated with Fe_3O_4 nanoparticles (SiO_2 gel/mag and fumed SiO_2/mag) were prepared to test the dependence of the photosensitizing activity of C_{60} on the host material. To prepare a silica support embedded with 40 wt% Fe_3O_4 nanoparticles, silica powder was slowly added to a solution of 6.97 g of $Fe(NO_3)_3{\cdot}9H_2O$ and 80 mL of ethanol with continuous stirring. After the solvent was evaporated at room temperature, the resulting powder was heated to 400 °C for 4 h under a flow of forming gas (4% H_2, 96% Ar) to generate a magnetic silica host. Next, 1 g of magnetic silica was suspended in a binary mixture of 1.5 mL of TPSA and 30 mL of toluene, and stirred for 24 h under argon protection. The resultant composite was filtered, washed with toluene, and subsequently dried at 60 °C, yielding 3-(2-succinic anhydride)propyl functionalized magnetic silica. The morphological features of the magnetic mesoporous silica and fullerene magnetic composites were investigated under a transmission electron microscope (TEM) (Jeol EM-2010, JEOL Co.) and a scanning electron microscope (SEM) (Jeol JSM-840A, JEOL Co.). Nitrogen adsorption/desorption isotherms were collected using a Micromeritics Tristar 3000 analyzer at 77 K. Powder X-ray diffraction (XRD) patterns were taken using a Bruker D8 Advance X-ray diffractometer with Cu Kα radiation. The stability of the bridge amide bond during the photosensitized singlet oxygenation was confirmed by X-ray photoelectron spectroscopy (XPS) (AXIS Ultra DLD, Kratos. Inc) using Al Kα lines (1486.6 eV) as an excitation source.

2.2. Photosensitized singlet oxygenation

Photosensitized oxidation reactions were conducted in a 30-mL Pyrex reactor with a quartz window under air-equilibrated conditions. A typical experimental suspension contained 0.3 g/L of a C_{60}-based magnetic photosensitizer and a 0.1 mM target substrate, and was buffered at pH 7 using 10 mM phosphate. Pre-irradiation with sonication for 1 min was performed to form an aqueous dispersion of the magnetic photosensitizer. The photolytic experiments were carried out using a 300-W Xe arc lamp (Oriel). Light was passed through a 10-cm IR water filter and a cut-off filter ($\lambda > 420$ nm). Next, 1 mL aliquots were withdrawn at predetermined time intervals from the photo-illuminated reactor using a 1 mL syringe, filtered through a 0.45-μm PTFE filter (Millipore), and injected into a 2-mL amber glass vial for further analysis. The residual concentrations of the target substrates including furfuryl alcohol (FFA) as an indicator for $^1O_2$ [26] and pharmaceutical compounds were monitored using an HPLC (Waters 2695) equipped with a C-18 column

(Nova-Pak C18) and a photodiode-array detector (Waters 996). The eluent consisted of a binary mixture of water and methanol (typically 60:40 by volume), while propranolol was quantitatively analyzed using a mobile phase comprising a mixture of water and acetonitrile (70:30 v/v).

2.3. Photo-induced viral inactivation

Disinfection experiments were performed using aqueous suspensions comprising a 0.3-g/L photosensitizer, 1.0×10^6 pfu/mL MS-2 bacteriophage (ATCC 15597), and 10 mM phosphate buffer. A 1-mL sample aliquot was collected following 15, 30, 45, 60, and 75 min of visible-light irradiation. The phage stock was prepared using soft agar overlay (double-agar layer) of confluent lysis and the viability of MS-2 phage was quantified by the soft agar overlay method with a plague assay using *Escherichia coli* (*E. coli*) C3000 as the host at the exponential to early stationary phase. Briefly, top and bottom agars were prepared with the addition of 7 and 15 g/L agar, respectively, in tryptone broth that contains 10 g/L tryptone, 8 g/L NaCl, 1 g/L yeast extract, 1 g/L glucose, and 0.22 g/L $CaCl_2$. The host *E. coli* C3000 was grown in tryptone broth for 18 h and recultured in a new broth for 4 h. 0.3 mL of diluted MS-2 phage sample and 0.1 mL of cultured *E. coli* were spiked onto 4.5 mL of soft agar, and the mixed agars were poured on top of the bottom agar. Plaques were counted after 24 h of incubation at 37 °C.

3. Results and discussion

3.1. Characteristics of functionalized magnetic silica

Table 1 lists the physical properties of magnetic silica supports (i.e., msu-SiO_2/mag, SiO_2 gel/mag, and fumed SiO_2/mag), which include the Brunauer–Emmett–Teller (BET) surface area, single point pore volume, cellular pore size, and Fe_3O_4 crystallite size. The pore size was calculated from a nitrogen adsorption/desorption isotherm by the Barrett–Joyner–Halenda (BJH) method (Supplementary data, Fig. S1a).

The incorporation of Fe_3O_4 nanoparticles in the pores of msu-SiO_2 caused a marked reduction in the BET surface area and pore volume (304.98 m^2/g (msu-SiO_2) compared to 183.59 m^2/g (msu-SiO_2/mag); 1.73 cm^3/g (msu-SiO_2) compared to 0.89 cm^3/g (msu-SiO_2/mag)). On the other hand, the pore size of msu-SiO_2 did not significantly vary before or after the encapsulation of the Fe_3O_4 nanoparticles (Supplementary data, Fig. S1b). In particular, a comparison with SiO_2 gel/mag and fumed SiO_2/mag (Table 1) suggests the presence of ultra-large pores in msu-SiO_2/mag.

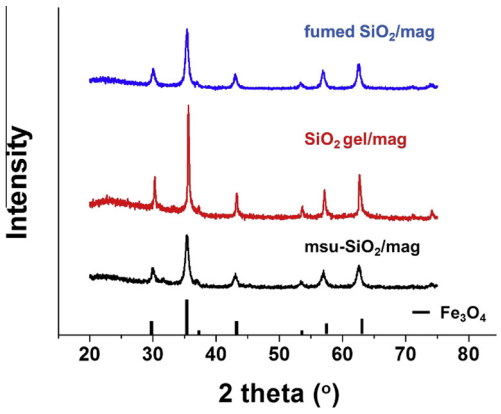

Fig. 1 – X-ray diffraction patterns of msu-SiO_2/mag, SiO_2 gel/mag, and fumed SiO_2/mag. (A colour version of this figure can be viewed online.)

The XRD peak patterns of msu-SiO_2/mag, SiO_2 gel/mag, and fumed SiO_2/mag are well-matched with those of a standard Fe_3O_4 crystal (JCPDS, 19-0629) (Fig. 1), confirming the formation of Fe_3O_4 on the magnetic silica by a wet impregnation method. Based on the Scherrer equation, the average crystallite diameters of Fe_3O_4 impregnated on msu-SiO_2, SiO_2 gel, and fumed SiO_2 were estimated to be 27.1, 69.08, and 33.89 nm, respectively (Table 1).

The TEM images of msu-SiO_2/mag revealed that the Fe_3O_4 nanoparticles are confined inside the pores of msu-SiO_2 (Fig. 2a and b). The fact that the crystallite sizes of the Fe_3O_4 nanoparticles are smaller than the sizes of the cellular pores of msu-SiO_2/mag also implies that the majority of Fe_3O_4 nanoparticles are encapsulated inside the pores of msu-SiO_2. The SEM images of msu-SiO_2/mag show that Fe_3O_4 particles are not present on the exterior surface and near the pore openings of msu-SiO_2 (Supplementary data, Fig. S2), further confirming successful incorporation of Fe_3O_4 into the mesopores.

In contrast to msu-SiO_2, the absence of an ordered pore structure of SiO_2 gel caused undesired aggregation of Fe_3O_4 nanoparticles (Fig. 2c). The intensive clustering of Fe_3O_4 nanoparticles on fumed SiO_2 might be inhibited by the confinement of Fe_3O_4 inside the interparticle pores of the 14-nm primary SiO_2 particles, which eventually sinter together to form SiO_2 aggregates (i.e., fumed SiO_2) with size ranging from

Table 1 – Physical properties of msu-SiO_2, msu-SiO_2/mag, SiO_2 gel/mag, and fumed SiO_2/mag, and crystallite sizes of Fe_3O_4 impregnated in SiO_2.

Sample	BET surface area (m^2/g)	Pore volume (cm^3/g)[a]	Pore diameter (nm)[b]	Crystallite size of Fe_3O_4 (nm)[c]
msu-SiO_2	304.98	1.73	43.19	N/A
msu-SiO_2/mag	183.59	0.89	44.90	27.10
SiO_2 gel/mag	274.82	0.37	7.00	69.08
fumed SiO_2/mag	114.94	0.51	N/A	33.89

[a] The pore volume was determined at $p/p_0 = 0.99$.
[b] The pore size distribution was calculated from the nitrogen isotherm by the BJH method.
[c] The crystallite size of Fe_3O_4 was calculated using the Scherrer equation.

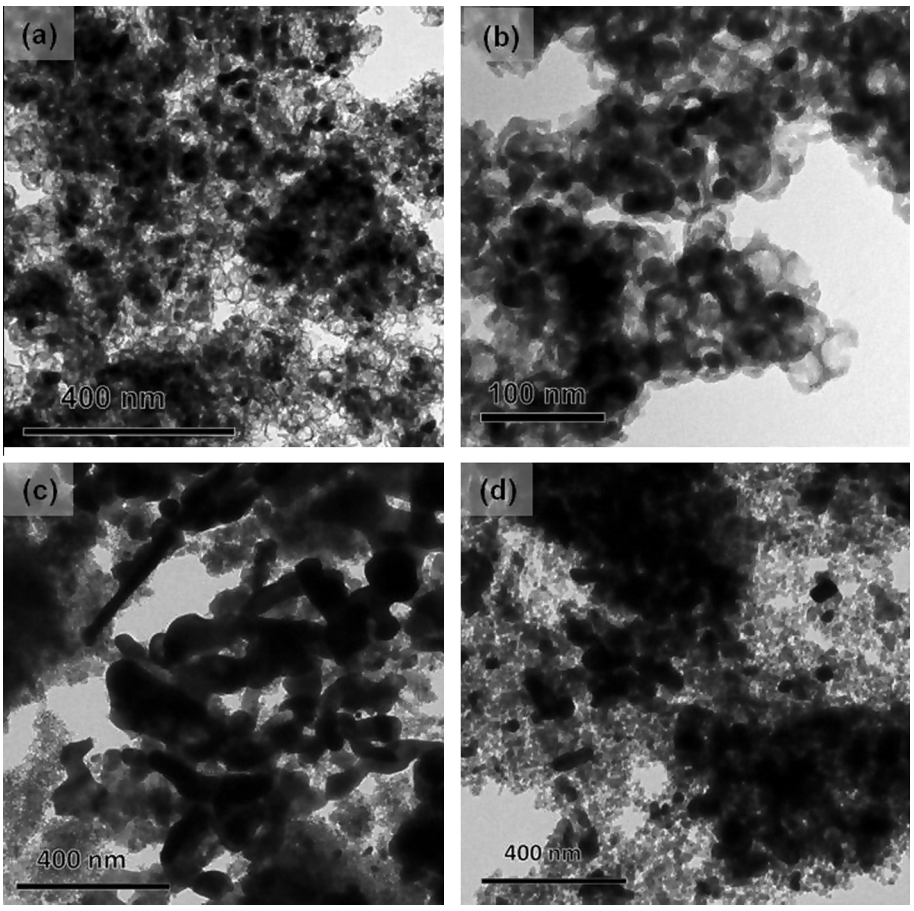

Fig. 2 – Transmission electron microscopy images of (a) and (b) msu-SiO_2/mag, (c) SiO_2 gel/mag, and (d) fumed SiO_2/mag.

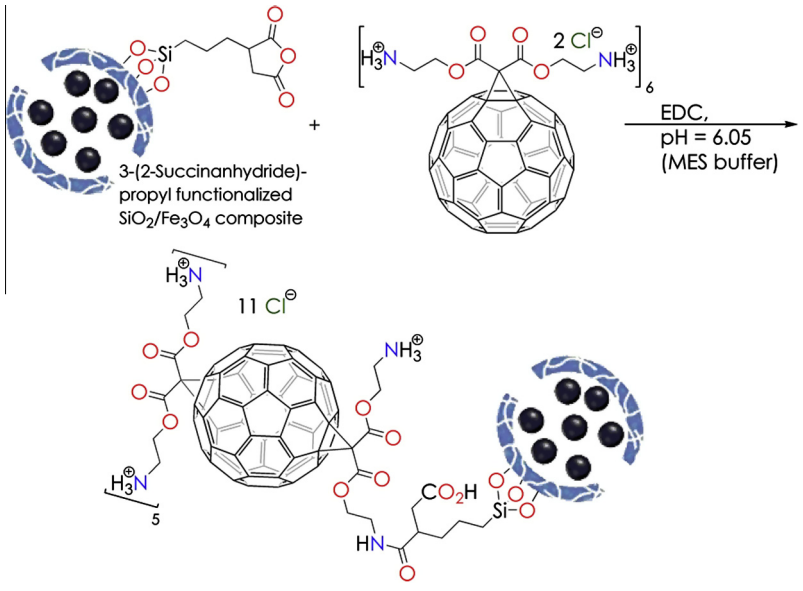

Fig. 3 – Immobilization of C_{60} aminofullerene on functionalized magnetic silica composite. (A colour version of this figure can be viewed online.)

200 to 300 nm [27]. However, Fe_3O_4 nanoparticles are present primarily outside of SiO_2 pores, which differ from msu-SiO_2/mag (Fig. 2d). Aggressive Fe_3O_4 clustering on SiO_2 gel and Fe_3O_4 formation outside of the pores of fumed SiO_2 will eventually result in a decreased photosensitizing activity, as discussed below.

3.2. Covalent bond-based immobilization of C_{60} photosensitizer

The immobilization of C_{60} aminofullerene (as a hydrochloride salt) on a magnetic silica support was performed according to our previously published procedure (Fig. 3) [18]. An amide bond linkage between C_{60} aminofullerene and 3-(2-succinic anhydride)propyl functionalized magnetic silica composite was produced using a water-soluble condensing reagent, N-(dimethylaminopropyl)-N′-ethylcarbodiimide hydrochloride (EDC). The optimal coupling conditions were achieved at room temperature in an aqueous solution, buffered at pH 6.05 with 0.1 M 2-(N-morpholino)ethanesulfonic acid (MES) hemisodium salt. The prepared fullerene-coated magnetic silica was separated from the suspension using a neodymium magnet, washed with distilled water and acetonitrile, and dried in a vacuum. Fourier transform infrared spectroscopy (FT-IR) patterns of the functionalized msu-SiO_2/mag before and after the surface loading of C_{60} aminofullerene confirmed the formation of an amide bond as an organic linker based on significant peaks at 1742 and 1679 cm^{-1} assigned to C=O (ester) and C=O (amide) (Supplementary data Fig. S3). Weight loss caused by the thermal decomposition of the organic moieties on the magnetic mesoporous silica, as measured using a thermogravimetric analyzer/differential scanning calorimeter (TGA/DSC), indicated that the aminofullerene content was 0.05 ± 0.01 mmol/g (Supplementary data, Fig. S4). Based on a comparison of the UV–visible reflectance spectra of msu-SiO_2/mag and C_{60}/msu-SiO_2/mag, the surface loading of C_{60} aminofullerene increased the visible-light absorption to a slight extent (Supplementary data, Fig. S5).

3.3. Photochemical $^1O_2$ production

The photosensitizing activity of C_{60}/msu-SiO_2/mag for $^1O_2$ generation was evaluated using the degradation of FFA as a chemical probe of $^1O_2$ [26] at a circumneutral pH under visible-light irradiation. Though a negligible FFA removal occurred with visible light irradiated msu-SiO_2/mag and C_{60}/msu-SiO_2/mag in the absence of light, the use of C_{60}/msu-SiO_2/mag caused a significant photochemical degradation of FFA (Fig. 4), which implies a key role of C_{60} aminofullerene in the oxidizing capacity of magnetically separable photosensitizer composites.

The involvement of $^1O_2$ in photochemical FFA oxidation by C_{60}/msu-SiO_2/mag was further verified based on the following observations. (1) The kinetic rate of FFA oxidation was markedly retarded in the presence of an excess amount of L-histidine acting as a $^1O_2$ scavenger. (2) The reduction in FFA concentration was accelerated when D_2O was alternatively employed as the solvent instead of H_2O, which can be ascribed to the reduced efficiency of D_2O for the solvent deactivation of $^1O_2$ relative to H_2O (i.e., $k_d(D_2O) = 1.6 \times 10^4\ s^{-1}$ versus $k_d(H_2O) = 2.4 \times 10^5\ s^{-1}$) (Fig. 4) [26].

3.4. Effect of magnetic silica support types

Fig. 4 also compares the photochemical $^1O_2$ production efficiency of C_{60}/msu-SiO_2/mag with that of C_{60}/SiO_2 gel/mag and C_{60}/fumed SiO_2/mag. SiO_2 gel/mag and fumed SiO_2/mag as a magnetic sensitizer support do not substantially differ from msu-SiO_2/mag in terms of the surface area (i.e., BET surface area (SiO_2 gel/mag) = 274.82 m^2/g; BET surface area (fumed SiO_2/mag) = 114.94 m^2/g; and BET surface area (msu-SiO_2/mag) = 183.59 m^2/g). Despite the surface coating with a similar amount of C_{60} aminofullerene, FFA was degraded 4- or 8-fold faster with C_{60}/msu-SiO_2/mag than C_{60}/fumed SiO_2/mag and C_{60}/SiO_2 gel/mag (i.e., $k = 1.33 \pm 0.17\ h^{-1}$ for C_{60}/msu-SiO_2/mag; $k = 0.306 \pm 0.008\ h^{-1}$ for C_{60}/fumed SiO_2/mag; and $k = 0.165 \pm 0.013\ h^{-1}$ for C_{60}/SiO_2 gel/mag) (Fig. 4), indicating the superiority of msu-SiO_2/mag as the immobilization support. The significantly lower photosensitizing activity of C_{60}/SiO_2 gel/mag and C_{60}/fumed SiO_2/mag is likely attributable to the absence of ordered pore structures entrapping Fe_3O_4 nanoparticles (confirmed in the XRD and TEM results). Electron energy loss spectroscopy (EELS) elemental mapping of C_{60}/msu-SiO_2/

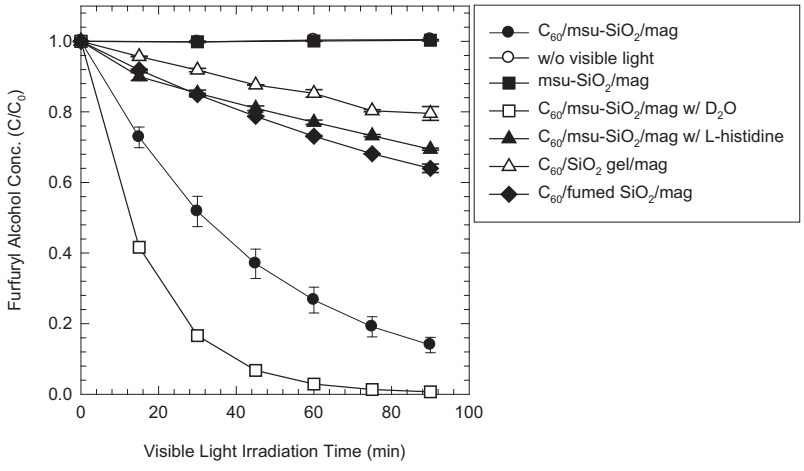

Fig. 4 – Degradation of furfuryl alcohol (as a probe test for photosensitized production of $^1O_2$) by C_{60}/msu-SiO_2/mag, C_{60}/SiO_2 gel/mag, and C_{60}/fumed SiO_2/mag under visible-light irradiation ([C_{60}-based photosensitizer]$_0$ = 0.3 g/L; [furfuryl alcohol]$_0$ = 0.1 mM; [L-histidine]$_0$ = 10 mM; [phosphate]$_0$ = 10 mM; and pH_i = 7.0).

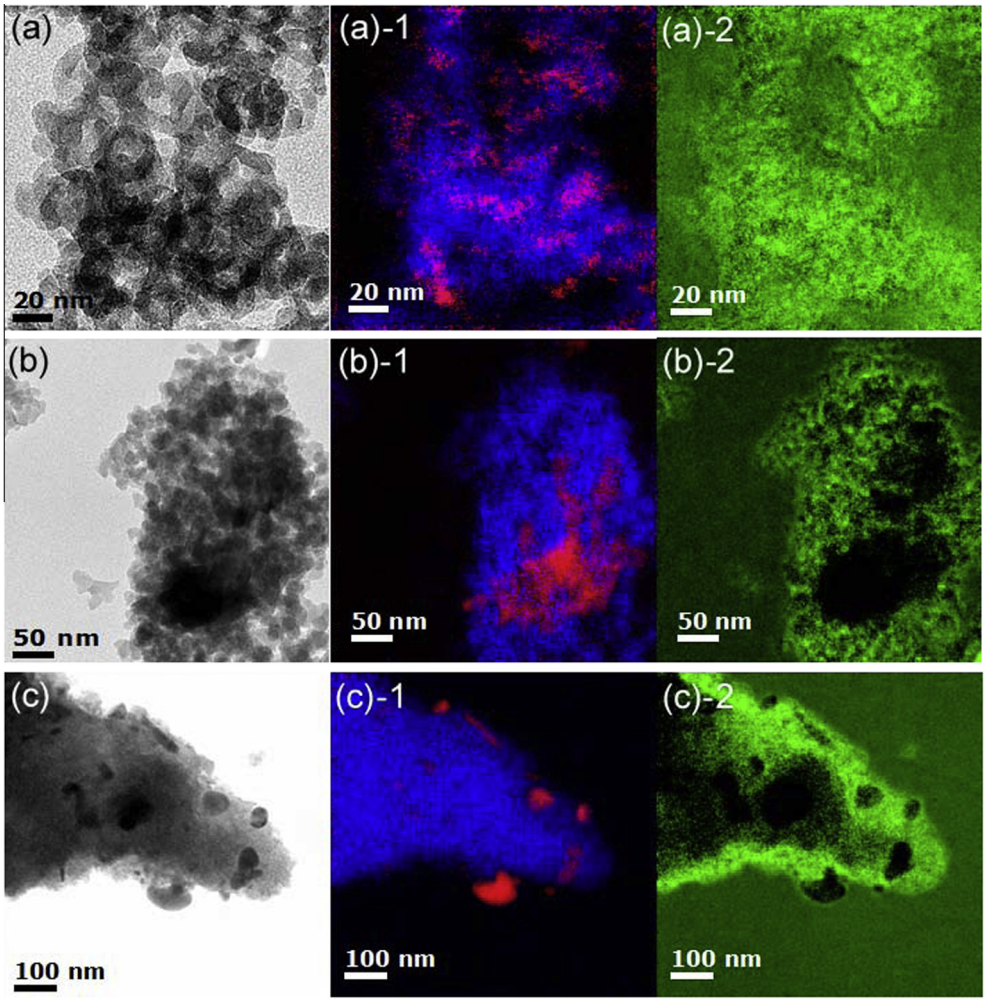

Fig. 5 – Electron energy loss spectroscopy (EELS) maps (obtained by JEM-2200FS microscope with Cs correction) and corresponding transmission electron microscopy images of C_{60} aminofullerene-magnetite composites. (a–c) Zero-loss filtering images of C_{60}/msu-SiO_2/mag, C_{60}/fumed SiO_2/mag, and C_{60}/SiO_2 gel/mag, respectively; and EELS maps of silicon and iron (blue, Si; red, Fe) ((a–c)-1) and carbon (green, C) ((a–c)-2). (A colour version of this figure can be viewed online.)

mag showed that Fe_3O_4 nanoparticles are encapsulated without significant clustering, and C_{60} aminofullerene is homogeneously dispersed over the msu-SiO_2 host (Fig. 5a). On the other hand, the spectroscopic mapping of iron and carbon on C_{60}/SiO_2 gel/mag and C_{60}/fumed SiO_2/mag revealed the aggregation of Fe_3O_4 nanoparticles, and the loading of C_{60} aminofullerene at spatially confined sites (Fig. 5b and c). The uncontrolled growth of Fe_3O_4 particles on the surface of SiO_2 gel and fumed SiO_2 hinders the uniform distribution of a succinic functional group (to form an organic linkage) on the support surface, which causes a localized C_{60} immobilization and eventually increases the chance of self-quenching and triplet–triplet annihilation to deactivate the sensitizers [14].

3.5. *Use of photoactive catalyst for $^1O_2$ yield*

To test the stability of a magnetic composite photocatalyst, photosensitized FFA oxidation with visible light was repeated over five cycles in aqueous suspensions of C_{60}/msu-SiO_2/mag (Fig. 6a). FFA degradation in each cycle was carried out in a separate batch using C_{60}/msu-SiO_2/mag, which was magnetically recovered after the end of each run of the photosensitized oxidation.

With a rapid separation from the suspension (Fig. 6b), the multiple use of C_{60}/msu-SiO_2/mag did not exhibit a significant reduction in the photosensitizing activity, which confirms the catalytic performance of the magnetic composite in $^1O_2$ production under visible-light irradiation. A successive decrease in the FFA removal rate observed after each cycle might be ascribed to the accumulation of FFA degradation intermediates that should also react with $^1O_2$. XPS spectra of freshly prepared and reused C_{60}/msu-SiO_2/mag (Supplementary data, Fig. S6) show that the N(1s) peak, as an indirect indication of amide linkage, remains after the photosensitized singlet oxygenation, which implies a low probability that C_{60}/msu-SiO_2/mag may undergo a loss of amide bonds through photogenerated $^1O_2$ and the associated release of the photoactive C_{60} moiety.

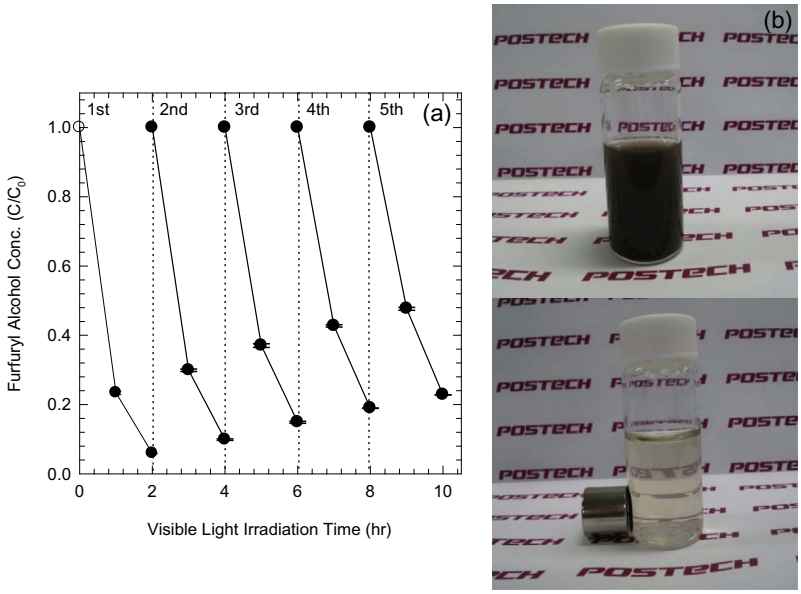

Fig. 6 – (a) Repeated cycles in the degradation of furfuryl alcohol by C_{60}/msu-SiO_2/mag under visible-light irradiation ([C_{60}/msu-SiO_2/mag]$_0$ = 0.3 g/L; [furfuryl alcohol]$_0$ = 0.1 mM; [phosphate]$_0$ = 10 mM; and pH_i = 7.0) and (b) demonstration of magnetic separation of C_{60}/msu-SiO_2/mag: aqueous dispersion of C_{60}/msu-SiO_2/mag (above) and separation of C_{60}/msu-SiO_2/mag with magnet after 4 min (below). (A colour version of this figure can be viewed online.)

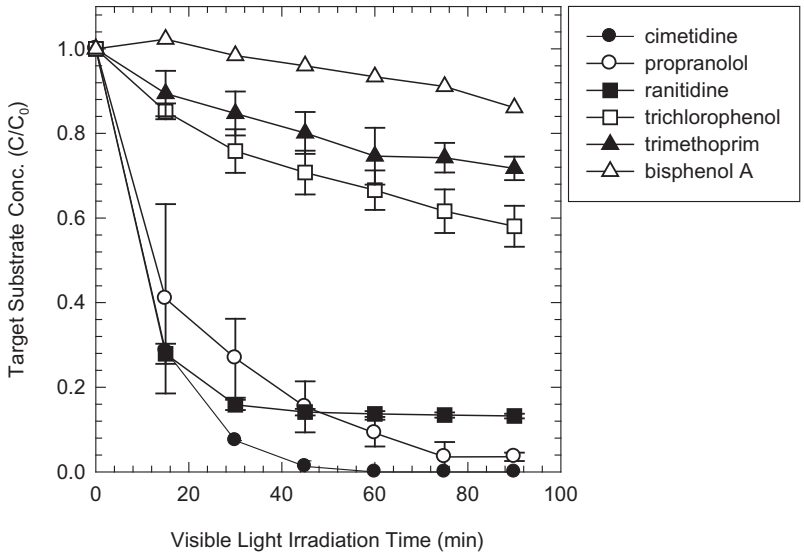

Fig. 7 – Photosensitized degradation of diverse organic compounds by C_{60}/msu-SiO_2/mag under visible-light irradiation ([C_{60}/msu-SiO_2/mag]$_0$ = 0.3 g/L; [target substrate]$_0$ = 0.1 mM; [phosphate]$_0$ = 10 mM; and pH_i = 7.0).

3.6. Photochemical pollutant oxidation and viral inactivation

The photochemical activity of C_{60}/msu-SiO_2/mag was examined for the oxidative degradation of several organic compounds including pharmaceuticals (i.e., cimetidine, propranolol, ranitidine, and trimethoprim) and phenols (i.e., trichlorophenol and bisphenol A) (Fig. 7). The kinetics for the photochemical degradation of organics is significantly dependent on the target substrate (Fig. 7), which is attributed to the selective nature of $^1O_2$ [28] as a primary oxidant in the C_{60}-mediated photosensitizing system. Owing to the high vulnerability of chemical moieties such as furan and imidazole to singlet oxygenation [28], C_{60}/msu-SiO_2/mag induced the rapid oxidation of cimetidine, propranolol, and ranitidine under visible-light illumination. On the other hand, the photochemical degradation of trimethoprim and trichlorophenol proceeded at relatively slow rates, and that of bisphenol A was not significant. In particular, the use of SiO_2 gel/mag and fumed SiO_2/mag as a magnetic catalyst support resulted in a drastic kinetic retardation in ranitidine oxidation (data not shown), which is compatible with ineffective FFA degradation

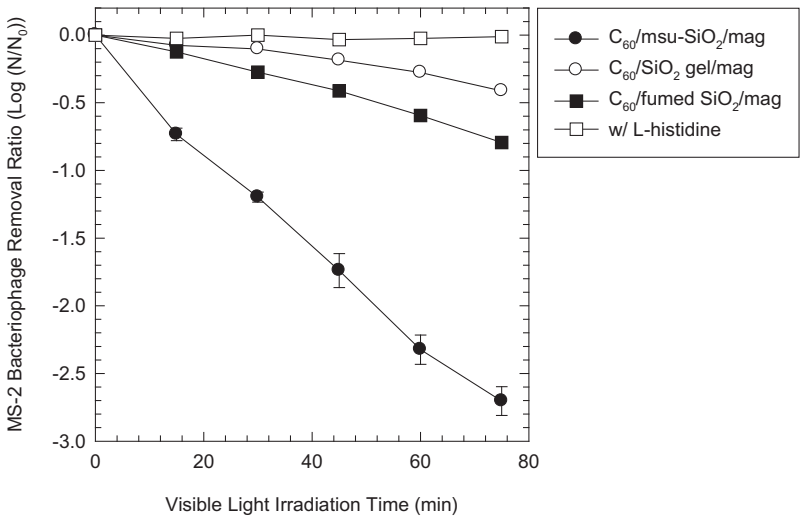

Fig. 8 – MS-2 bacteriophage inactivation by C_{60}/msu-SiO_2/mag, C_{60}/SiO_2 gel/mag, and C_{60}/fumed SiO_2/mag under visible-light irradiation ([C_{60}-based photosensitizer]$_0$ = 0.3 g/L; [MS-2 bacteriophage]$_0$ = 1.0×10^6 pfu/mL; [L-histidine]$_0$ = 10 mM; [phosphate]$_0$ = 10 mM; and pH_i = 7.0).

(indirect indication for $^1O_2$ formation) during the photo-irradiation of C_{60}/SiO_2 gel/mag and C_{60}/fumed SiO_2/mag (Fig. 4).

Photochemically generated $^1O_2$ from the aqueous suspensions of C_{60}/msu-SiO_2/mag was also applied for the disinfection of MS-2 bacteriophage. Whereas either direct photolysis or sorption under dark conditions caused a negligible removal of the MS-2 bacteriophage (data not shown), C_{60}/msu-SiO_2/mag efficiently inactivated the MS-2 bacteriophage with visible light (Fig. 8). In the presence of excess L-histidine (a scavenger of $^1O_2$), the viral inactivation was completely inhibited, which supports the predominant role of $^1O_2$ as the main disinfectant. In particular, rates for photosensitized removal of MS-2 bacteriophage in suspensions of C_{60}/msu-SiO_2/mag, C_{60}/SiO_2 gel/mag, and C_{60}/fumed SiO_2/mag (C_{60}/msu-SiO_2/mag ($k = 5.22\ h^{-1}$) > C_{60}/fumed SiO_2/mag ($k = 1.38\ h^{-1}$) > C_{60}/SiO_2 gel/mag ($k = 0.672\ h^{-1}$) were quantitatively correlated to the photochemical activities for $^1O_2$ production (Fig. 4), which further verifies the critical involvement of photoproduced $^1O_2$ in C_{60}-mediated viral inactivation.

4. Conclusion

In this work, we developed a magnetically recoverable visible-light-responsive photosensitizer. For the proposed photosensitizer, C_{60} aminofullerene was covalently immobilized on the functionalized mesoporous silica encapsulating Fe_3O_4 nanoparticles in its cellular pores. The high yield production of $^1O_2$ by the magnetic fullerene sensitizer was confirmed using FFA as a probe. The magnetic composite photocatalyst enabled the oxidative degradation of the selected organic pollutants and inactivation of MS-2 bacteriophage under visible-light irradiation; its oxidation activity is dependent on the type of substrate, which is ascribed to the selective nature of the singlet oxygen activity. The overgrowth of Fe_3O_4 and localized loading of C_{60} aminofullerene on SiO_2 gel and fumed SiO_2 markedly reduced the efficiency of $^1O_2$ production from the magnetic C_{60} composites, which indicates that the confinement of Fe_3O_4 nanoparticles within the cellular pores of mesoporous silica is critical to achieving the maximal photosensitization activity. No significant reduction in the photosensitizing capacity or magnetic separation efficiency was observed during the repeated test cycles, which demonstrated the practical applicability of the composite photocatalyst. The combination of magnetic and visible-light-responsive properties enables a rapid sensitizer recovery without an external energy supply, as well as the potential application of solar energy for water treatment and disinfection processes.

Acknowledgements

This study was supported by the Korea Institute of Science and Technology (KIST) Institutional Program (2E22853) and the KIST Global Research Laboratory Project (2Z03740). Partial funding was also provided by the Robert A. Welch Foundation (Grant C-0627), the Korea National Research Foundation (Korean Ministry of Education, Science and Technology (NRF-2011-35B-D00020), the "The GAIA Project" (No. 2012000550021) of the Korea Ministry of Environment, and the "Converging Technology Project" of the Korea Ministry of Environment, as funded by KIST (2011000600001).

Appendix A. Supplementary data

Supplementary data associated with this article can be found, in the online version, at http://dx.doi.org/10.1016/j.carbon.2013.11.065.

REFERENCES

[1] Leary R, Westwood A. Carbonaceous nanomaterials for the enhancement of TiO_2 photocatalysis. Carbon 2011;49:741.

[2] Park Y, Singh NJ, Kim KS, Tachikawa T, Majima T, Choi W. Fullerol-titania charge-transfer-mediated photocatalysis working under visible light. Chem Eur J 2009;15:10843.
[3] Tajima T, Sakata W, Wada T, Tsutsui A, Nishimoto S, Miyake M, et al. Photosensitized hydrogen evolution from water using a single-walled carbon nanotube/fullerodendron/SiO_2 coaxial nanohybrid. Adv Mater 2011;23:5750.
[4] Zhang XY, Li HP, Cui XL, Lin YH. Graphene/TiO_2 nanocomposites: synthesis, characterization and application in hydrogen evolution from water photocatalytic splitting. J. Mater. Chem. 2010;20:2801.
[5] Arbogast JW, Darmanyan AP, Foote CS, Rubin Y, Diederich FN, Alvarez MM, et al. Photophysical properties of C_{60}. J Phys Chem 1991;95:11.
[6] Vileno B, Sienkiewicz A, Lekka M, Kulik AJ, Forro L. In vitro assay of singlet oxygen generation in the presence of water-soluble derivatives of C_{60}. Carbon 2004;42:1195.
[7] Yamakoshi Y, Umezawa N, Ryu A, Arakane K, Miyata N, Goda Y, et al. Active oxygen species generated from photoexcited fullerene (C_{60}) as potential medicines: $O_2^{\cdot-}$ versus $^1O_2$. J Am Chem Soc 2003;125:12803.
[8] Ruoff RS, Tse DS, Malhotra R, Lorents DC. Solubility of C_{60} in a variety of solvents. J Phys Chem 1993;97:3379.
[9] Andrievsky GV, Kosevich MV, Vovk OM, Shelkovsky VS, Vashchenko LA. On the production of an aqueous colloidal solution of fullerenes. J Chem Soc Chem Commun 1995:1281.
[10] Beeby A, Eastoe J, Heenan RK. Solubilization of C_{60} in aqueous micellar solution. J Chem Soc Chem Commun 1994:173.
[11] Lee J, Mackeyev Y, Cho M, Li D, Kim JH, Wilson LJ, et al. Photochemical and antimicrobial properties of novel C_{60} derivatives in aqueous systems. Environ Sci Technol 2009;43:6604.
[12] Richardson CF, Schuster DI, Wilson SR. Synthesis and characterization of water-soluble amino fullerene derivatives. Org Lett 2000;2:1011.
[13] Hotze EM, Labille J, Alvarez P, Wiesner MR. Mechanisms of photochemistry and reactive oxygen production by fullerene suspensions in water. Environ Sci Technol 2008;42:4175.
[14] Lee J, Kim JH. Effect of encapsulating agents on dispersion status and photochemical reactivity of C_{60} in the aqueous phase. Environ Sci Technol 2008;42:1552.
[15] Cho M, Lee J, Mackeyev Y, Wilson LJ, Alvarez PJJ, Hughes JB, et al. Visible light sensitized inactivation of MS-2 bacteriophage by a cationic amine-functionalized C_{60} derivative. Environ Sci Technol 2010;44:6685.
[16] Badireddy AR, Hotze EM, Chellam S, Alvarez P, Wiesner MR. Inactivation of Bacteriophages via photosensitization of fullerol nanoparticles. Environ Sci Technol 2007;41:6627.
[17] Chae SR, Hotze EM, Wiesner MR. Evaluation of the oxidation of organic compounds by aqueous suspensions of photosensitized hydroxylated-C_{60} fullerene aggregates. Environ Sci Technol 2009;43:6208.
[18] Lee J, Mackeyev Y, Cho M, Wilson LJ, Kim JH, Alvarez PJJ. C_{60} aminofullerene immobilized on silica as a visible-light-activated photocatalyst. Environ Sci Technol 2010;44:9488.
[19] Oberdorster E, Zhu SQ, Blickley TM, McClellan-Green P, Haasch ML. Ecotoxicology of carbon-based engineered nanoparticles: Effects of fullerene (C_{60}) on aquatic organisms. Carbon 2006;44:1112.
[20] Usenko CY, Harper SL, Tanguay RL. In vivo evaluation of carbon fullerene toxicity using embryonic zebrafish. Carbon 2007;45:1891.
[21] Lee J, Hong S, Mackeyev Y, Lee C, Chung E, Wilson LJ, et al. Photosensitized oxidation of emerging organic pollutants by tetrakis C_{60} aminofullerene-derivatized silica under visible light irradiation. Environ Sci Technol 2011;45:10598.
[22] Deng Y, Qi D, Deng C, Zhang X, Zhao D. Superparamagnetic high-magnetization microspheres with an Fe_3O_4@SiO_2 core and perpendicularly aligned mesoporous SiO_2 shell for removal of microcystins. J Am Chem Soc 2008;130:28.
[23] Kim J, Piao Y, Hyeon T. Multifunctional nanostructured materials for multimodal imaging, and simultaneous imaging and therapy. Chem Soc Rev 2009;38:372.
[24] Kim MI, Shim J, Li T, Lee J, Park HG. Fabrication of nanoporous nanocomposites entrapping Fe_3O_4 magnetic nanoparticles and oxidases for colorimetric biosensing" as the article title. Chem Eur J 2011;17:10700.
[25] Kim SS, Pauly TR, Pinnavaia TJ. Non-ionic surfactant assembly of ordered, very large pore molecular sieve silicas from water soluble silicates. Chem Commun 2000:1661.
[26] Haag WR, Hoigné J. Singlet oxygen in surface waters. 3. Photochemical formation and steady-state concentrations in various types of waters. Environ Sci Technol 1986;20:341.
[27] Bakaev VA, Pantano CG. Inverse reaction chromatography. 2. Hydrogen/Deuterium exchange with silanol groups on the surface of fumed silica. J Phys Chem C 2009;113:13894.
[28] Wilkinson F, Helman WP, Ross AB. Rate constants for the decay and reactions of the lowest electronically excited singlet state of molecular oxygen in solution - An expanded and revised compilation. J Phys Chem Ref Data 1995;24:663.